

Provided for non-commercial research and education use.
Not for reproduction, distribution or commercial use.



This article appeared in a journal published by Elsevier. The attached copy is furnished to the author for internal non-commercial research and education use, including for instruction at the authors institution and sharing with colleagues.

Other uses, including reproduction and distribution, or selling or licensing copies, or posting to personal, institutional or third party websites are prohibited.

In most cases authors are permitted to post their version of the article (e.g. in Word or Tex form) to their personal website or institutional repository. Authors requiring further information regarding Elsevier's archiving and manuscript policies are encouraged to visit:

<http://www.elsevier.com/copyright>



Contents lists available at ScienceDirect

Composites: Part A

journal homepage: www.elsevier.com/locate/compositesa

Wireless strain measurement for structural testing and health monitoring of carbon fiber composites

Federico Gasco^a, Paolo Feraboli^{a,*}, Jeff Braun^{b,c}, Joshua Smith^{b,c}, Patrick Stickler^d, Luciano DeOto^e

^a Automobili Lamborghini Advanced Composite Structures Laboratory, Dept. of Aeronautics & Astronautics, University of Washington, Seattle, WA 98195-2400, United States

^b Dept. of Electrical Engineering University of Washington, Seattle, WA, United States

^c Intel Research Labs., Seattle, WA, United States

^d Boeing 787 Airframe Service Ready Team, Boeing Commercial Airplanes, Everett, WA, United States

^e Advanced Composites Research Center, Automobili Lamborghini S.p.A., Sant'Agata Bolognese, Italy

ARTICLE INFO

Article history:

Received 10 January 2011

Received in revised form 27 April 2011

Accepted 7 May 2011

Available online 14 May 2011

Keywords:

A. Carbon fiber

B. Smart structures

D. Mechanical testing

Sensors

ABSTRACT

A novel device patented by Intel and called WISP (Wireless Identification and Sensing Platform) is modified to interface with a conventional foil resistance strain gage. The wireless, battery-free, digital device communicates with and is powered by an Ultra-High Frequency (UHF) RFID (Radio Frequency Identification) reader. The standard Intel WISP has been modified with the addition of a PCB (printed circuit board), which act as the analog interface with the strain gage. The so-called WISPs/g (for strain gage) has been utilized during uniaxial tension tests on carbon fiber composite specimens to compare accuracy and repeatability with conventional wired strain gage and extensometer. Validation of the technology is performed with a structural test, whereby four independent WISPs/g devices are positioned on the surface of a carbon fiber composite flat panel subjected to quasi-static indentation. Measurements are compared to the predictions of a NASTRAN finite element model (FEM) and show excellent agreement. Applications of this technology include strain measurement during static airframe tests, as well as on-board real-time strain measurements during test flight and certification of new aircraft.

© 2011 Elsevier Ltd. All rights reserved.

1. Introduction

Strain measurement is a critical component during aircraft certification. It is used to measure the strain at critical locations during tests at all levels of the building block, from the coupon level (for example to measure material modulus), through the element and subcomponent level (for example to measure strain distributions during compression testing of stiffened panels with damage), and up to the full-scale level (for example to measure limit load and ultimate load strains at critical locations to validate analytical model predictions). Unfortunately, for each strain gage used it is often necessary to utilize long, costly and cumbersome electrical wires that connect the gage to the data acquisition board and then to the computing device for data processing. The possibility to utilize wireless devices to measure strain is therefore highly sought-after in the aerospace community.

Several examples of wireless strain sensors can be found in the literature. However, the majority consists of analog devices, based on antenna resonance frequency [1] and capacitive strain gauges [2]. Analog technology is appealing because it requires low-power supply, unlike digital technology, which is not very power-effi-

cient. However, analog devices are known to have poor repeatability due to the variability in measurements associated with environmental conditions (moisture, temperature, electromagnetic interference (EMI), etc.) and often provide inconsistent measurements. Furthermore, analog devices are often tied to extensive application-specific calibration, and therefore lack in flexibility of use. Recent development in Micro-Electro-Mechanical Systems (MEMS) have enabled the advent of other battery-free wireless strain sensors [3,4]. However, MEMS devices utilize non-conventional methods to measure strain, are usually very expensive, and in general they are not application-ready. In recent years, low-power microprocessors have enabled the design of digital wireless strain sensors that are commercially available. The sensors developed by Microstrain Inc. [5–8] provide analog-to-digital data acquisition and conversion, have low-power programmable microcontroller, and utilize radio frequency (RF) bidirectional data link. Strain measurement is provided by conventional foil resistance strain gage, which is a proven technology. However, the devices [5,6] are powered by a Lithium battery pack, which has a long yet limited service life. In [5] a beam-bending test is performed and strain is measured with ± 2.5 microstrain of accuracy over a range of 4000 microstrain. In [6], the device is used to measure strain during static testing of the Lockheed F/A-22, and it is shown to be compatible with the metallic test frame environment and with

* Corresponding author.

E-mail address: feraboli@aa.washington.edu (P. Feraboli).

the composite airframe EMI. Very successful results are reported in terms of accuracy, number of strain gages supported and transmission distance. In [7,8] the Microstrain Inc. sensor platform was modified with the addition of piezoelectric energy harvesters, which can power the device and recharge the Lithium battery. In [7] the authors simulated the strain spectrum for the rotor of a NAVY Blackbird helicopter in the laboratory, and demonstrated continuous operation of the sensor at a minimum strain sampling rate of 40 Hz without any battery for energy storage. The successful installation of this sensor on a Bell M412 helicopter is documented in [8].

The device developed in this paper combines all the advantages of the devices described in the literature. It features wireless and digital transmission, it is battery-free, and utilizes conventional strain-gage technology as the measurement sensor. The research discussed in the following sections is based on the WISP device, introduced and patented by Intel in 2007 [9,10], which is modified to interface with a foil resistive strain gage. After a brief summary of the electronic architecture and functioning of the WISP device, discussed at length in [9,10], the paper discusses the modifications that are needed to interface the device with a conventional strain gage. These modifications include the addition of a printed circuit board (PCB), which is comprised of an amplifier and Wheatstone bridge. The WISPs/g, so named because of the presence of the strain gage and interface PCB, is then calibrated to the gain of the selected resistive strain gage. Following the one-time calibration, the device is then used for uniaxial tension tests of carbon fiber composite specimens to compare accuracy and repeatability with a conventional wired strain gage and an extensometer. To prove the validity of the approach, four independent WISPs/g devices are used to monitor the real-time deformation of a carbon fiber composite panel undergoing structural testing under complex loading. The panel is subjected to through-thickness indentation in the center of the panel as well as in two offset positions, and the strain gage measurements are used to measure the strain on the surface of the panel. Measurements are then compared to the predictions of a NASTRAN finite element model (FEM). Lastly, a roadmap is discussed that shows how the WISPs/g can be transferred from its current PCB design to an integrated circuit (IC) design. This modification would enable the manufacturing of stand-alone, single-use WISPs/g devices supported on a polymeric substrate, similar to conventional RFID tags, which are ideal for mass production and are very inexpensive.

2. Intel WISP device

The WISP device (Fig. 1) receives its power and communicates through a UHF RFID reader. RFID is a well-known technology that features an integrated circuit for modulating and demodulating a radio-frequency signal, and an antenna for transmitting and receiving the signal. RFID tags are widely used as transponders with applications in inventory tracking and management, and can be manufactured both in PCB and IC forms. Like conventional RFID tags, the WISP receives and rectifies RF energy to power its onboard circuitry, and communicates with the Reader Antenna through a technique called backscatter radiation. Unlike

conventional RFID tags, which transmit only a fixed identification number, the WISP encodes data using an ultra-low-power programmable microcontroller. Each ID sent from the WISP includes data that can be subsequently extracted and analyzed.

The key features of the WISP are the wireless, battery-free power supply through RF, bidirectional RF communication with backscatter uplink, and a fully programmable ultra-low-power microcontroller with an analog-to-digital converter (ADC). The ADC offers the possibility to integrate low-power sensors that can be used for remote querying. Several types of sensors, like temperature, ambient light and acceleration sensors have been successfully integrated in the WISP PCB [10]. The functional block diagram of the WISP is shown in Fig. 2. A personal computer (PC) connected to the RFID reader through local network protocols is used to execute the RFID reader software. The RFID reader converts these software commands into a signal that can be transmitted to the WISP. The RF signal is transmitted through an 8 dBi circularly polarized Reader Antenna, which establishes a wireless power and data link (915 MHz) with the WISP. The WISP is powered solely by the RF harvested from its antenna, which has a range [10] up to 14.8 ft. (4.5 m). The RF signal that is absorbed by the Antenna is passed through an impedance matching network (Fig. 3) in order to minimize reflection loss. The signal is then split into two paths, one used to power the WISP, and one for data transmission. The first path proceeds to a power harvester, which is comprised of a rectifier and a storage capacitor, and then onto a voltage regulator and a voltage supervisor. The voltage regulator ensures that the voltage supplied by the harvester does not overload the microcontroller, while the voltage supervisor monitors the voltage level of the storage capacitor and activates the microcontroller when that level reaches the required value. The second signal path goes through the demodulator, which transforms the RF-modulated signal to a digital signal, which enables the microcontroller to interpret the data transmitted by the reader. After executing its preprogrammed firmware (built-in software), the microcontroller transmits the data to a modulator, which converts the digital information into RF-modulated signal. This return signal, which contains the data processed by the WISP, is received by the Reader Antenna and sent onto the RFID reader, which interprets the signal and sends it back to the PC for subsequent data analysis. The frequency of power and data exchange between the WISP Antenna and the Reader Antenna decreases with range. In particular, the RF power decreases with the square of the distance from the Reader Antenna [9,10]. Therefore distance between the WISP and the Reader Antenna needs to be selected as a compromise between performance (sampling rate) and space requirements.

The microcontroller is a Texas Instrument 16-bit flash MSP430, which has very low power requirements because it is kept in stand-by except when activated. The WISP continuously harvests RF energy and collects it in the capacitor, while the microcontroller is in sleep mode. When sufficient energy is accumulated, the voltage supervisor sends a signal to the microcontroller and activates it. The microcontroller executes its firmware, which consists of activating the external sensor power and converting its output from analog to digital through the built-in 10-bit ADC. The ADC converts it to an analog signal to collect data from the external sensor, and then converts it back to digital format and sends it

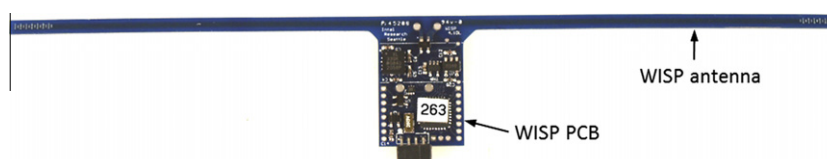


Fig. 1. Intel WISP. (For interpretation of the references to color in this figure legend, the reader is referred to the web version of this article.)

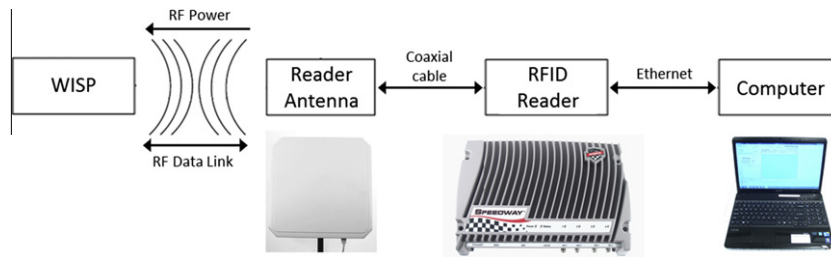


Fig. 2. WISP querying and reading system functional diagram. (For interpretation of the references to color in this figure legend, the reader is referred to the web version of this article.)

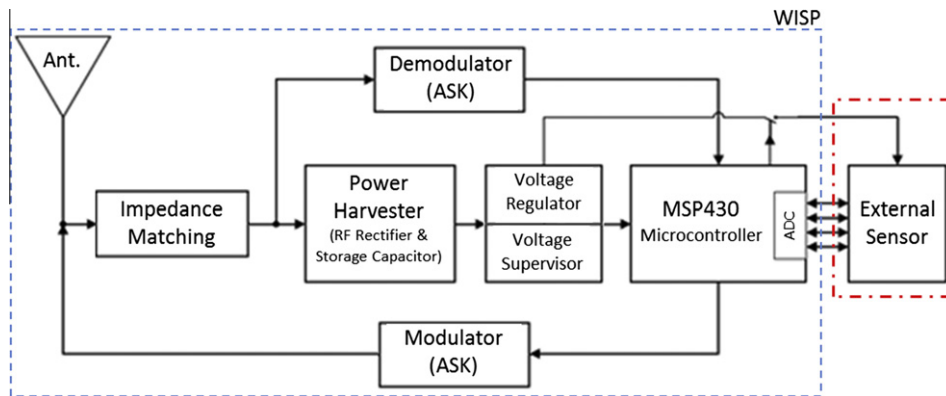


Fig. 3. WISP functional block diagram [10]. (For interpretation of the references to color in this figure legend, the reader is referred to the web version of this article.)

to the microcontroller. Multiple external sensors can be connected and queried by a single WISP device. At this point the data packet contains the sensor data and ID information, and is known as EPC (electronic product code) identifier.

A detailed view of the top (front) side of the WISP is shown in Fig. 4. The antenna, which is not shown, is attached to the two pins on the far right. The microcontroller is shown in the center-left portion of the PCB, while the socket used to connect the WISP to a PC for programming is shown on the far left. At the periphery of the left side of the WISP are a series of pins that can be used to connect multiple sensors. The ones used in this study to connect the strain gage and associated PCB, which will be discussed below, are indicated as GND, P3.0 and P3.5. In particular, the pin labeled GND is the ground,

the pin labeled P3.5 is used to power and excite the sensor, and the pin labeled P3.0 is used to measure the sensor output.

3. WISPs/g for strain measurement applications

In order to interface the WISP with the strain sensor, which has additional power requirements, an additional circuit has been designed and built on a PCB, and it is hereinafter referred to as the strain gage PCB (SGPCB), Fig. 5. The SGPCB is comprised of the Wheatstone bridge, which converts the resistance change of the strain gage into a voltage change, and of the amplifier, which increases the intensity of the voltage change. The WISP provides

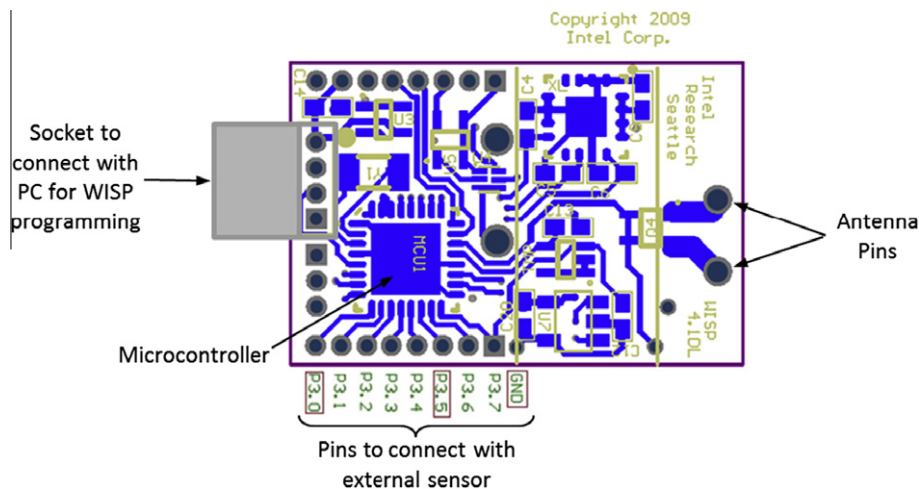


Fig. 4. Top view of the WISP PCB layout showing the principal electrical components (antenna not shown). (For interpretation of the references to color in this figure legend, the reader is referred to the web version of this article.)

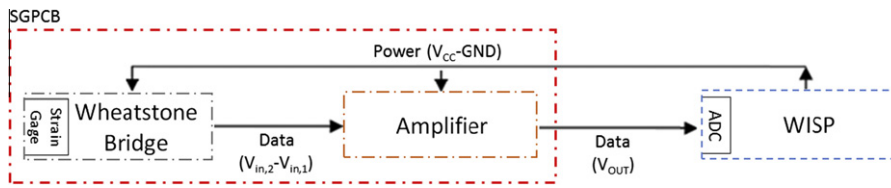


Fig. 5. WISPs/g sensor power and signal conditioning block diagram. (For interpretation of the references to color in this figure legend, the reader is referred to the web version of this article.)

power to both the amplifier and the Wheatstone bridge. The Wheatstone bridge relays the strain gage voltage to the amplifier, which transmits it as analog signal to the ADC. The strain sensor is a uniaxial general purpose foil resistance strain gage (Omega SGD-13/1000-LY11) with 1000 Ω resistance, gage factor (GF) of 2.0 and active gage length of 0.5 in. (12.7 mm). This high resistance strain gage is selected to reduce power consumption. The SGPCB and strain gage are shown in Fig. 6. From this point on, the overall system comprised of the WISP, SGPCB and strain gage is referred to as the WISPs/g.

The electrical diagram of the SGPCB is shown in Fig. 7, and includes the Wheatstone bridge and strain gage (left) and the

amplifier (right). The Wheatstone bridge is comprised of four segments, each characterized by one or more resistors. Resistors R_1 , R_2 , R_3 , and R_4 have a fixed resistance. The strain gage has a variable resistance R_{SG} , which changes with the applied strain. The resistor R_4 is placed in series with R_{SG} to reduce the current consumption of the circuit without significantly degrading the Signal to Noise Ratio (SNR) performance. The power consumption of the amplifier circuit is measured using a DC power supply to be 2.71 mW at the peak value of excitation voltage (2.5 V). The average power consumption of the WISP alone (without the SGPCB) when active is 1.08 mW [10]. Although the power consumption of the circuit could be reduced by using smaller resistors, the SNR would be

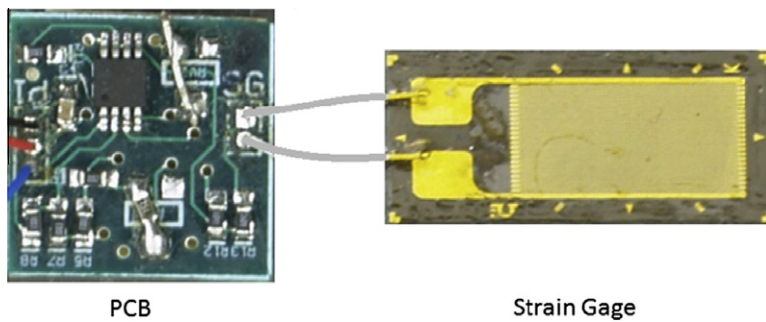


Fig. 6. The system comprised of the SGPCB and conventional strain gage is designed to interface with the WISP of Fig. 1 to form the WISPs/g. (For interpretation of the references to color in this figure legend, the reader is referred to the web version of this article.)

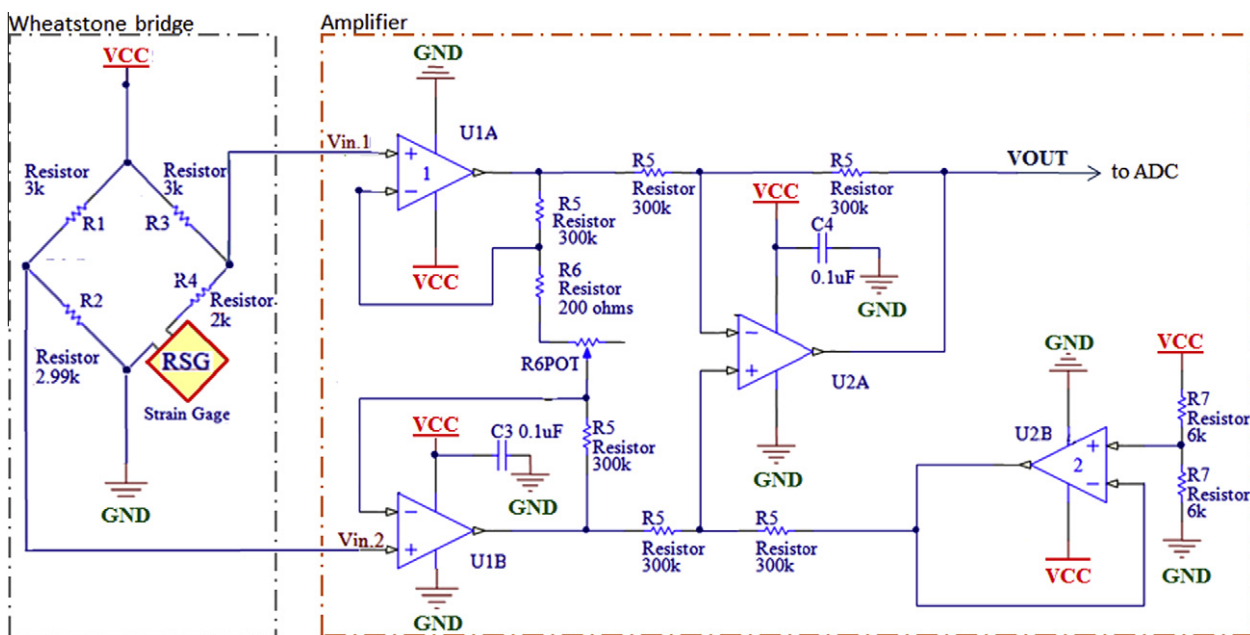


Fig. 7. Schematic of the SGPCB, showing the Wheatstone bridge on the left (which also includes the strain gage) and the signal amplifier on the right. (For interpretation of the references to color in this figure legend, the reader is referred to the web version of this article.)

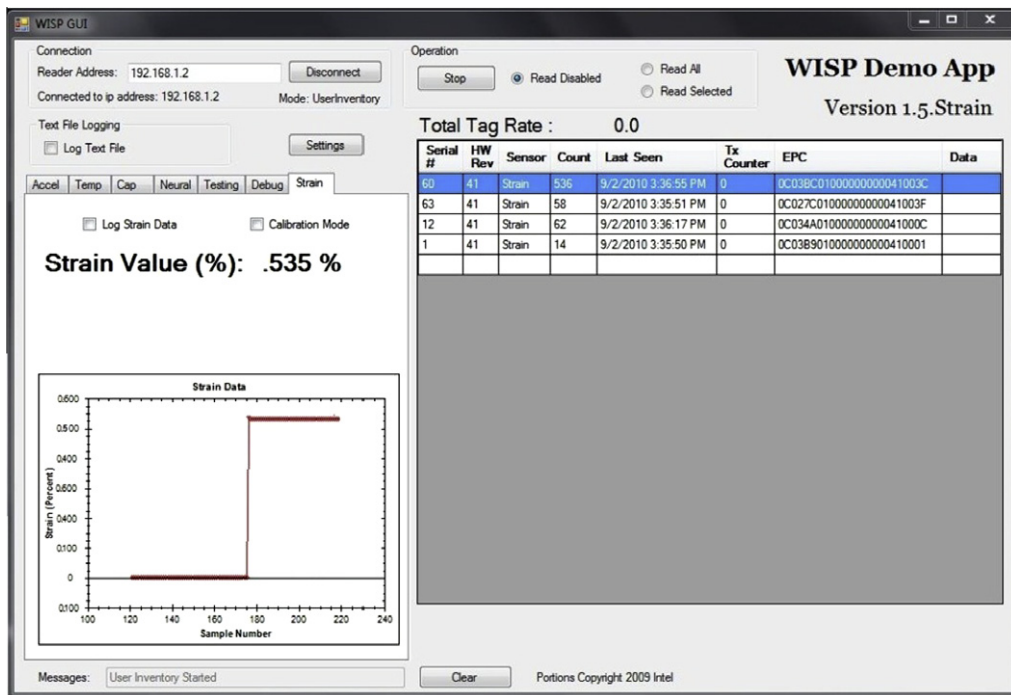


Fig. 8. WISPs/g reader software interface during reading mode. The load step applied in a tension test is associated to the strain step plotted on display. (For interpretation of the references to color in this figure legend, the reader is referred to the web version of this article.)



Fig. 9. Tension test specimen with WISPs/g device, showing from left to right the WISP, the SGPCB, and the conventional strain gage. (For interpretation of the references to color in this figure legend, the reader is referred to the web version of this article.)

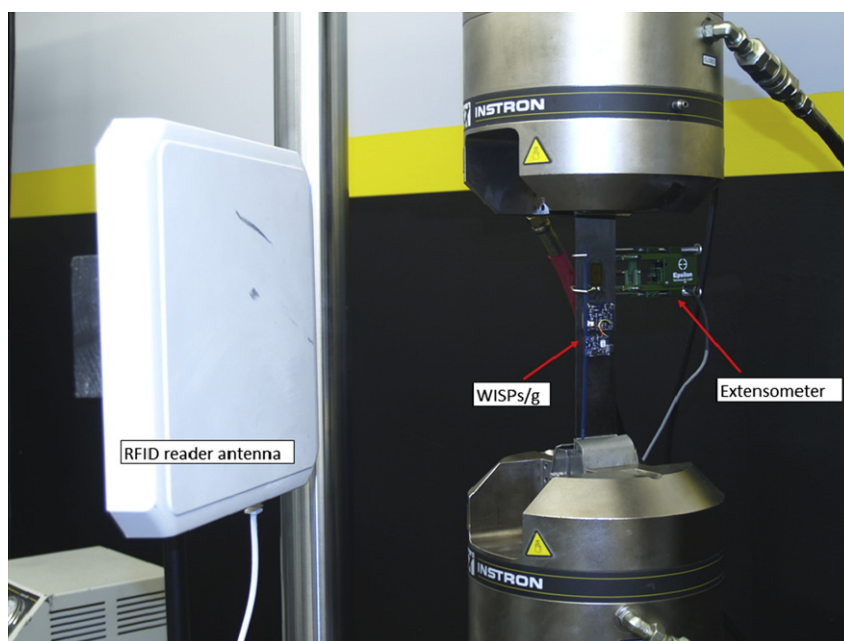


Fig. 10. Tension test setup, showing the specimen in the test frame (with the WISPs/g, the extensometer and the wired strain gage) and the powering RFID antenna reader. (For interpretation of the references to color in this figure legend, the reader is referred to the web version of this article.)

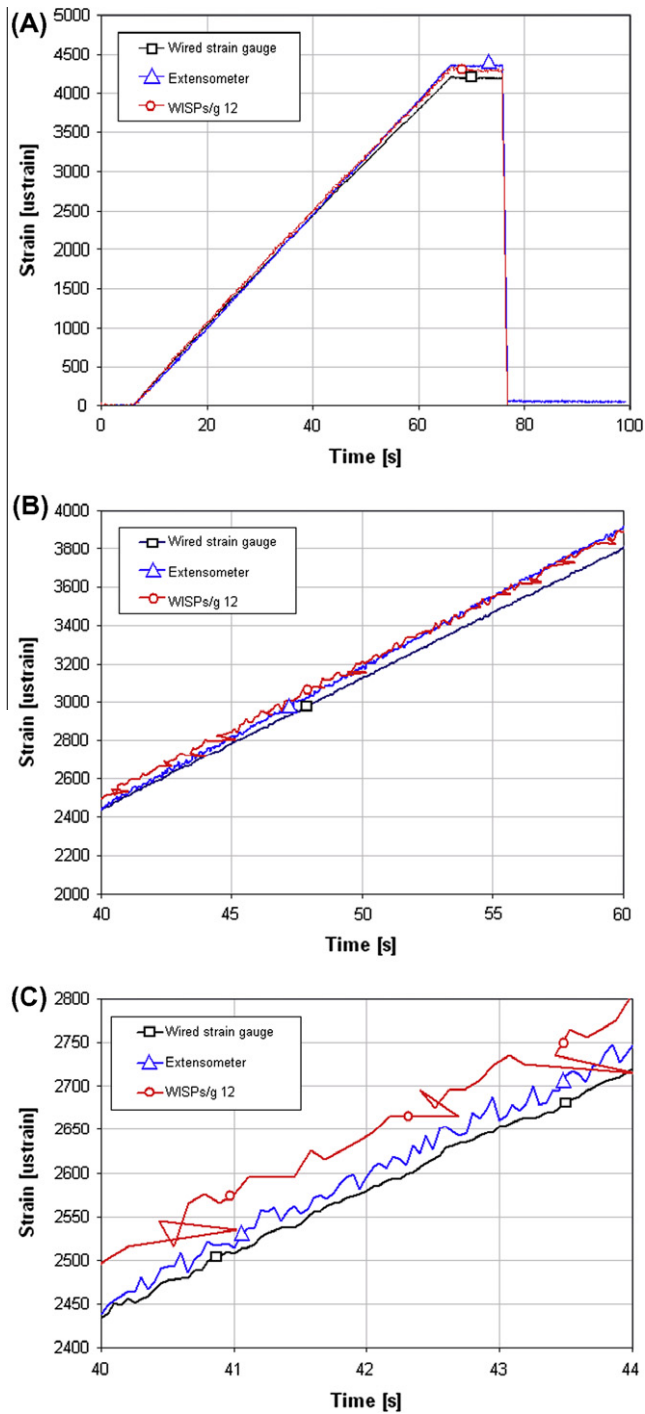


Fig. 11. (A–C) Ramp load tension test curves, as measured with the WISPs/g and calibrated against the wired strain gauge and extensometer (A), and details of the curves showing noise (B) and periodic time-shift in a single data point. (For interpretation of the references to color in this figure legend, the reader is referred to the web version of this article.)

reduced as well. The value of resistance has to be chosen as a compromise between SNR and power consumption.

There are eight connections marked as GND in Fig. 7, each of which is connected to the GND pin of Fig. 4. Similarly, there are six connections marked as V_{CC} , which are connected to the 3.5 pin of Fig. 4, and are used to deliver power from the WISP to the amplifier and strain gage. The single connection marked as V_{OUT} is tied to the 3.0 pin of Fig. 4, and it is used to transfer the strain gage measurement data to the ADC of the WISP.

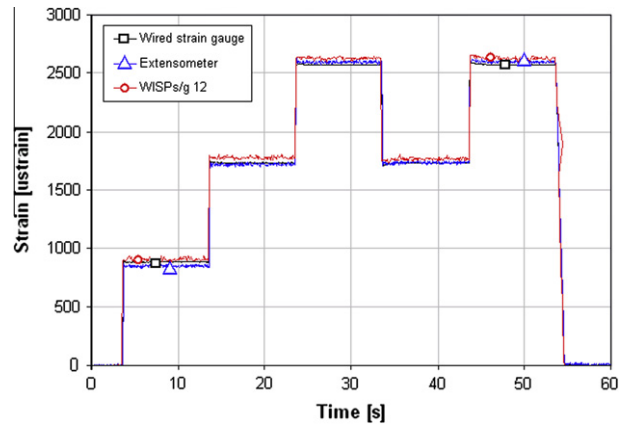


Fig. 12. Step load tension test curves, as measured with the WISPs/g and calibrated against the wired strain gauge and extensometer. (For interpretation of the references to color in this figure legend, the reader is referred to the web version of this article.)

The resistance of the strain gage R_{SG} is given by:

$$R_{SG} = R_{SG,0} + GFR_{SG,0}\varepsilon \quad (1)$$

where ε is the instantaneous value of the strain measured by the strain gage, GF is the fixed gage factor (2.0 for the strain gage used in this study), and $R_{SG,0}$ is the resistance of the strain gage at zero strain (1000 Ω for the strain gage used in this study). The Wheatstone bridge provides two outputs: $V_{in,1}$, which is the variable input for the amplifier, and $V_{in,2}$, which remains constant and is a reference voltage level. When the gage senses a strain, the value of R_{SG} changes and the voltage $V_{in,1}$ changes as well. The output of the bridge, $V_{in,2} - V_{in,1}$, is the input for the amplifier:

$$V_{in,2} - V_{in,1} = \left(\frac{R_2}{R_1 + R_2} - \frac{R_4 + R_{SG}}{R_3 + R_4 + R_{SG}} \right) V_{CC} \quad (2)$$

where $V_{CC} = 1.8$ V and is the excitation voltage that the WISP applies to the bridge.

The amplifier is comprised of four different operational amplifiers, U1A, U2A, U1B and U2B, which together are responsible for the amplification of the voltage signal and act as buffers for the impedance matching.

The output of the entire circuit, V_{OUT} , passes through the ADC of the microcontroller. V_{OUT} is given by:

$$V_{OUT} = (V_{in,2} - V_{in,1}) \left(1 + \frac{2R_5}{R_6 + R_{6,POT}} \right) \quad (3)$$

The potentiometer $R_{6,POT}$, which is variable resistor, is used to adjust the gain of the entire circuit during a one-time calibration, which will be discussed later. The values of the resistors are defined in Fig. 7, i.e. $3k = 3000 \Omega$. The output of the ADC is given by:

$$ADC = \frac{1024V_{OUT}}{V_{CC}} \quad (4)$$

where V_{OUT} and V_{CC} have been previously defined, and 1024 is the maximum number that can be expressed in the binary numbering system using the 10 bits available. The resolution of the device can be found by dividing the maximum strain (previously defined to be 10,000 microstrain) by the 1024 discrete levels of the ADC, which gives approximately a ± 5 microstrain accuracy (or less than $\pm 0.2\%$ for 3000 microstrain).

The WISPs/g needs to be calibrated to a specific strain gage in terms of offset and sensitivity. Regulating the potentiometer $R_{6,POT}$ in the amplifier allows for changing the voltage output for a given applied strain, thus increasing the sensitivity of the

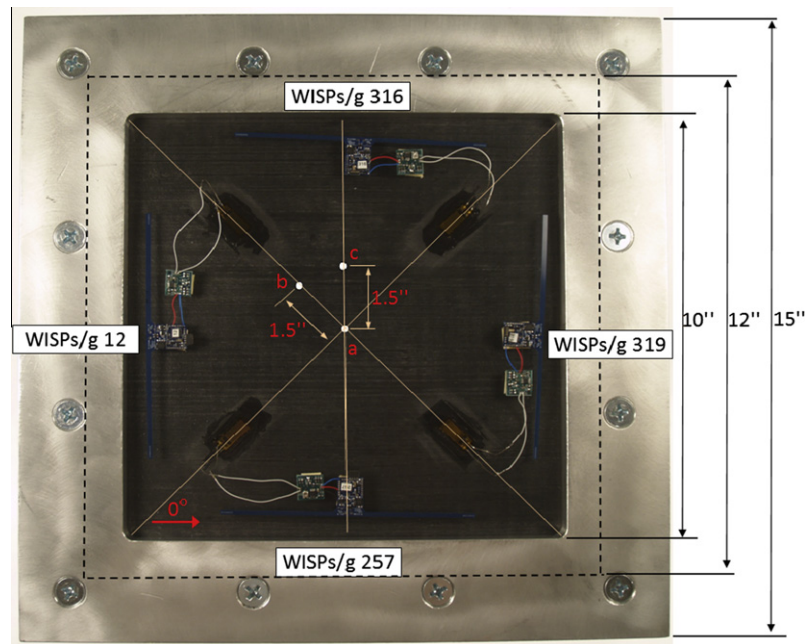


Fig. 13. Quasi-static indentation fixture and panel dimensions, also showing the location and alignment of the four WISPs/g devices with associated strain gages. Indentation test performed by moving the indenter to three locations: (a) center load; (b) offset load in the 45° (WISPs/g #12) direction; (c) offset load (between WISPs/g #12 and #319). (For interpretation of the references to color in this figure legend, the reader is referred to the web version of this article.)

measurement. The voltage output needs to be sufficiently sensitive and not reach saturation up to the maximum value of strain to be measured, which is set to be 10,000 microstrain. From Eq. (4), it can be seen that if at any point in the test the condition were to occur where $V_{OUT} \geq V_{CC}$, the ADC output would saturate and the measurement would be lost. For a single strain gage type, with a given resistance and gage factor, a one-time calibration of the amplifier is performed by conducting a tension test with a WISPs/g. Since all WISPs/g devices are identical, the calibration needs to be conducted only on a single device if the strain gages utilized are identical as well, i.e. they have the same resistance and gage factor. For the 1000 Ω strain gage utilized, $R_{6,POT}$ has been set to 750 Ω following the one-time calibration.

Similar to wired strain gages, the zero strain offset needs to be set prior to each measurement, regardless if the same strain gage and WISP is utilized. Through the software, developed to interface the user with the WISPs/g, it is possible to set the zero-strain value for each test. The software can be opened in calibration mode and testing mode. The calibration mode allows the user to define the zero strain offset and to input the strain gage gain factor based on the specifications of the strain gage. This software calibration must be performed every time the WISPs/g is operated, prior to testing, similar to traditional wired strain measurement. The software reports in real time the serial number, sensor name ("strain"), total number of ID readings, date and time of last ID reading and EPC for each of the WISPs/g that have been seen by the reader (Fig. 8). If a WISPs/g is located within the range of the RFID Reader Antenna, it is automatically detected by the software and it begins transmission of data. In the testing mode, the strain value is displayed and plotted in real-time, and the strain data is stored in text file.

4. Validation of the WISPs/g

4.1. Tension testing

The WISPs/g, comprised of the WISP and the SGPCB, is bonded onto a carbon fiber composite specimen using traditional methods.

Since carbon fiber is conductive, it has non-negligible RF properties. In particular, carbon fiber reduces significantly the strength of the antenna signal, and if the WISP is left in contact or close-proximity to the carbon fiber surface, it has reduced transmission capability [11,12]. The resistivity of carbon fiber composites ranges from about 10^{-2} to 10^{14} depending on the properties of the composite, such as fiber volume fraction. This is a very wide resistivity range and extends well into a region of conductivity that is high enough to absorb a significant amount of the RF signal. Therefore, using double-sided tape, the WISP is raised 0.25 in. (6.35 mm) from the surface of the specimen to improve the communication with RFID Reader Antenna and insulate it electrically. This practice does not influence the strain gage, which is bonded using common practices to the surface of the specimen. Future work will be aimed at designing a wireless antenna that can better tolerate the EMI of the carbon fiber substrate and can yield improved RF performance of the system.

The specimen is comprised of IM7/977-3 carbon fiber/epoxy unidirectional prepreg tape, having a stacking sequence of $[0/90]_{3s}$ for a thickness of 0.085 in. (2.2 mm). The laminate is cured at 350 F (177 C) and 85 psi (5.9 bar) for 2.5 h (the cure cycle is the C-49 with reduced isothermal hold) by press molding in a heated press using match-mold aluminum dies. The specimen is a straightedge ASTM D3039 tension test specimen, Fig. 9, of dimensions 12 in. (305 mm) \times 1.5 in. (38 mm). Material properties provided by the supplier are ply thickness 0.0075 in. (0.19 mm), $E_1 = 23.5$ Msi (162 GPa), $E_2 = 1.21$ Msi (8.34 GPa), and $G_{12} = 0.72$ Msi (5.0 GPa), $\nu_{12} = 0.34$. Two tension tests for each WISPs/g are performed, one with a step-function load and one with a ramp load. All tests are performed in the elastic region (strain measurement in the range 1000–4500 microstrain). Evaluation of the WISPs/g and associated strain gage is performed against the measurements obtained by a single identical wired strain gage and a 1.0 in. (25.4 mm) gage-length extensometer. Four WISPs/g, denoted as #12, #257, #316, and #319, are tested using the same carbon fiber composite specimen and the same bonded strain gage. These are tested to check the variability of the response among the devices, in particular the accuracy and the noise of the strain

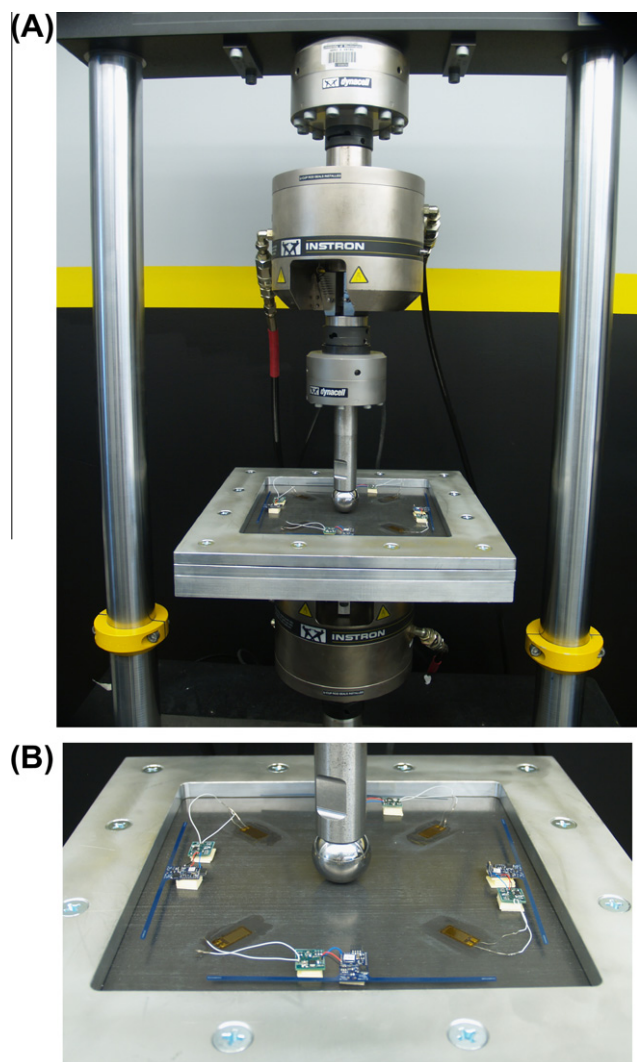


Fig. 14. (A and B) Two views of the quasi-static indentation test setup. (For interpretation of the references to color in this figure legend, the reader is referred to the web version of this article.)

measurements. These same four devices are later used in a quasi-static indentation test, which is discussed in the following section. Tests are performed in an Instron Universal test frame under displacement control, using hydraulic grips to clamp the specimen. The RF communication and power transfer from the Reader Antenna to the WISP are affected by EMI of the universal test frame machine and grips surrounding the test area. These metal components are longer than 6.3 in. (160 mm), which is the half-wavelength of the operating frequency of the RFID communication system (915 MHz). These electrically-long metal sections act as antennas and absorb some of the RF signal and also reflect some of the RF energy back into the air. This phenomenon interferes with the communications between the WISP and the antenna reader, hence the distance between the two has to be dramatically reduced. It is found that for these tests, the RFID Reader Antenna needs to be kept within 2 ft (0.6 m) from the WISP. The test setup is shown in Fig. 10.

Typical results are shown in Figs. 11A–C and 12. The WISPs/g strain is in good agreement with the data collected with the extensometer and the wired strain gage, which means that the response of the WISPs/g is linear and the slope is consistent. Periodically during a tension test, there may be a time-shift in a single, random data point within the strain–time curve, Fig. 11B and C. These

random occurrences are associated to a minor “bug” in the reader software that records the strain data together with the corresponding CPU time. Nonetheless, since 10–20 data points are collected per second, a single data point shift does not affect the global measurement in a non-dynamic test. Further work would resolve this issue with small changes to the software. The WISPs/g exhibits a slightly larger amount of high-frequency noise compared to the wired measurements, Figs. 11 and 12. The primary source of noise is probably due to inconsistencies of the strain gauge amplifier power voltage. The WISPs/g does not have enough incident RF power to indefinitely power itself and the strain gauge, therefore it duty cycles its operations to store energy. This duty cycling leads to an inconsistency in the operating voltage level. The strain gauge amplifier circuit has a capacitor across its voltage rails to help combat this voltage inconsistency, but there may be still variance in the voltage level at which the measurement is taken. However additional investigation on the hardware and on the firmware of the WISPs/g is needed to understand the reasons of this noise. Nevertheless the noise observed is negligible in the context of the strain region typical of a quasi-static test, where data is average over a wide range of strain. Note that the time resolutions of each of the three methods of measurement are different. The wired strain gauge has the highest resolution, the extensometer’s read rate is in the middle, and the WISPs/g has the slowest read rate. The time resolutions of the extensometer and the wired strain gauge are fixed and are determined by the settings of the data acquisition equipment used to log their data. In contrast, the WISPs/g time resolution is variable and is limited by its power budget.

4.2. Quasi-static indentation testing

In order to verify the ability of the WISPs/g to accurately measure complex strain states, a quasi-static indentation test of a flat composite panel is performed. The material, laminate stacking sequence, and cure cycle of the panel are the same as the tension specimen. This type of test is typically utilized in damage resistance and tolerance studies to inflict damage for subsequent residual strength testing [13–15]. The test fixture, resembling a square picture frame, has outer dimensions of 15 in. (381 mm) and an inner aperture (unsupported span) of 10 in. (254 mm), Fig. 13. The same fixture can be utilized also for low-velocity impact damage testing using a drop tower. The panel edges are supported between the upper and lower portions of the fixture, which in turn are clamped together by bolts. The panel is trimmed to 12 in. (304.8 mm), thus providing 1.0 in. (25.4 mm) of overhang on each side, which is clamped between the upper and lower portions of the fixture. The panel in-plane displacement at the edges is constrained only by friction, which is function of the bolt tightening torque.

Previous research [13–15] has shown that such supports should be idealized as simply supported boundary conditions (b.c.), since clamped b.c. tend to overestimate the degree of stiffness of the set-up. The fixture assembly is held in position through a bracket to the lower grip of the universal test machine, while the indenter is held in position by the upper grip of the universal test machine, Fig. 14A and B. A spherical indenter of 1.0 (25.4 mm) diameter is used to apply the load. The sphere is held in position through a semicircular seat inside the load actuator, which allows it to self-align. Four WISPs/g devices are placed on the panel and supported as in the case of the tension specimen. Each WISPs/g is connected to a single 0.5 in. (12.7 mm) strain gage, whose longitudinal direction is oriented at 45° from the 0 direction of the panel, and oriented toward the center of the plate. All four gages are equidistant from the center of the panel long the diagonals, at a distance of 3.5 in. (90 mm), Figs. 13 and 14B. Three different loading conditions are evaluated, Fig. 15. Load case (a) is a centered load, which

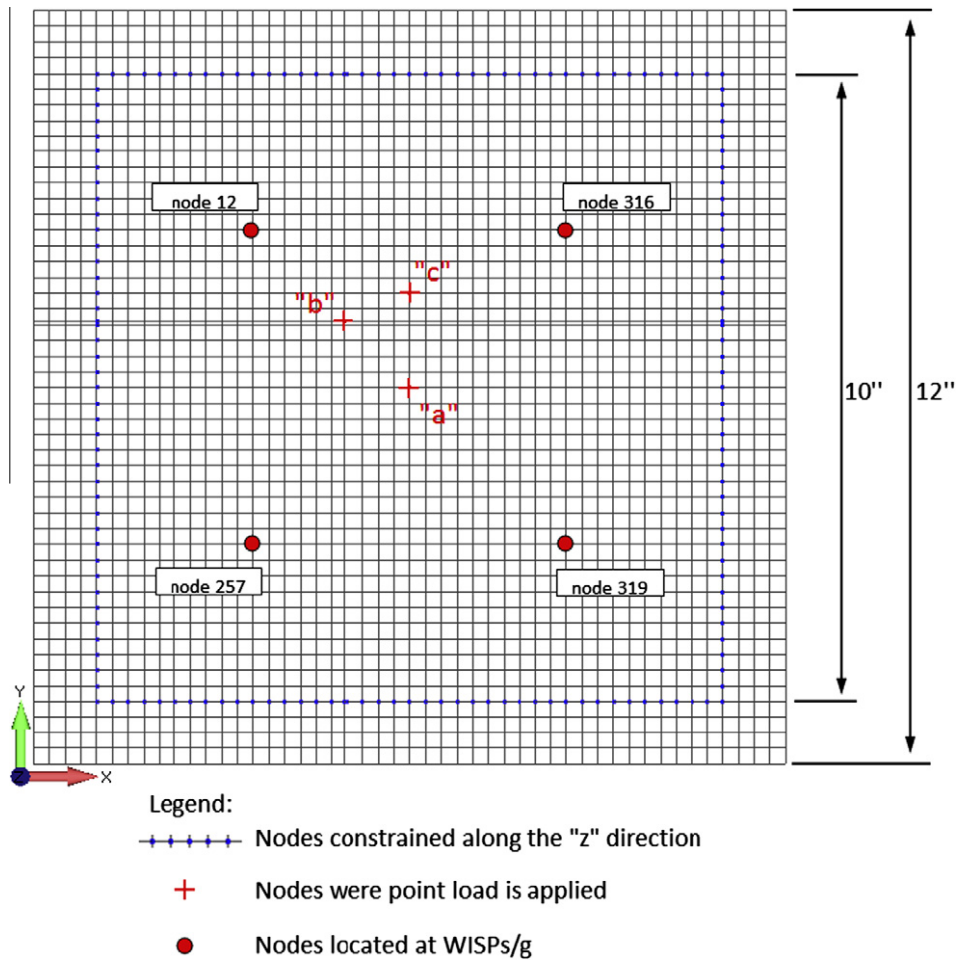


Fig. 15. NASTRAN nonlinear finite element model of quasi-static indentation test, also showing the location of the four WISPs/g devices (with homonymous node locations), boundary conditions and applied load. Simulated indentation test performed by moving the point load to three locations: (a) center load; (b) offset load in the 45° (WISPs/g #12) direction; (c) offset load (between WISPs/g #12 and #319). (For interpretation of the references to color in this figure legend, the reader is referred to the web version of this article.)

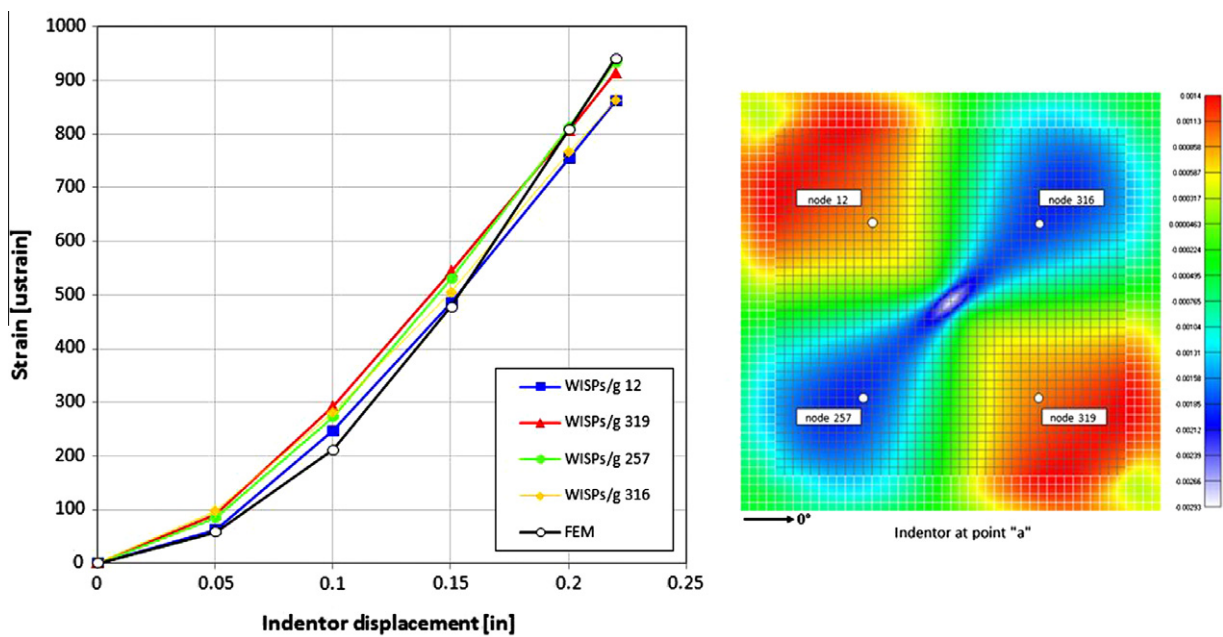


Fig. 16. (Left) Experimental and simulated strain curves for all four gages as a function of indenter displacement for the load case (a). (Right) Strain contour plot from the simulation for the same load case. (For interpretation of the references to color in this figure legend, the reader is referred to the web version of this article.)

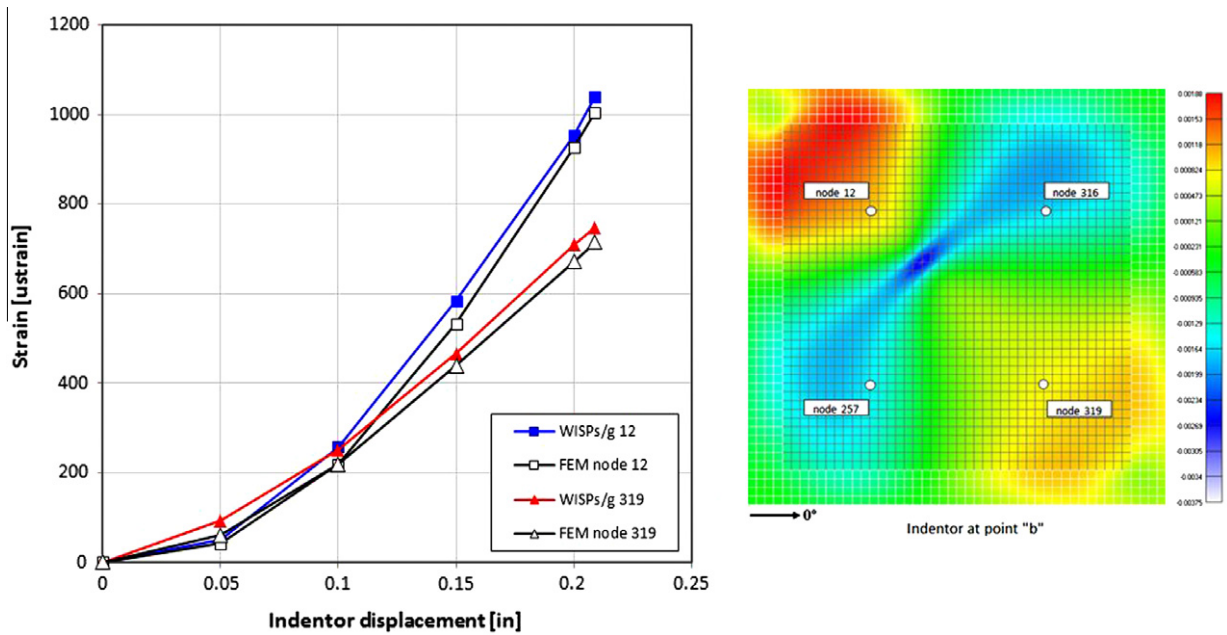


Fig. 17. (Left) Experimental and simulated strain curves for gages #12 and #319 as a function of indentor displacement for the load case (b). (Right) Strain contour plot from the simulation for the same load case. (For interpretation of the references to color in this figure legend, the reader is referred to the web version of this article.)

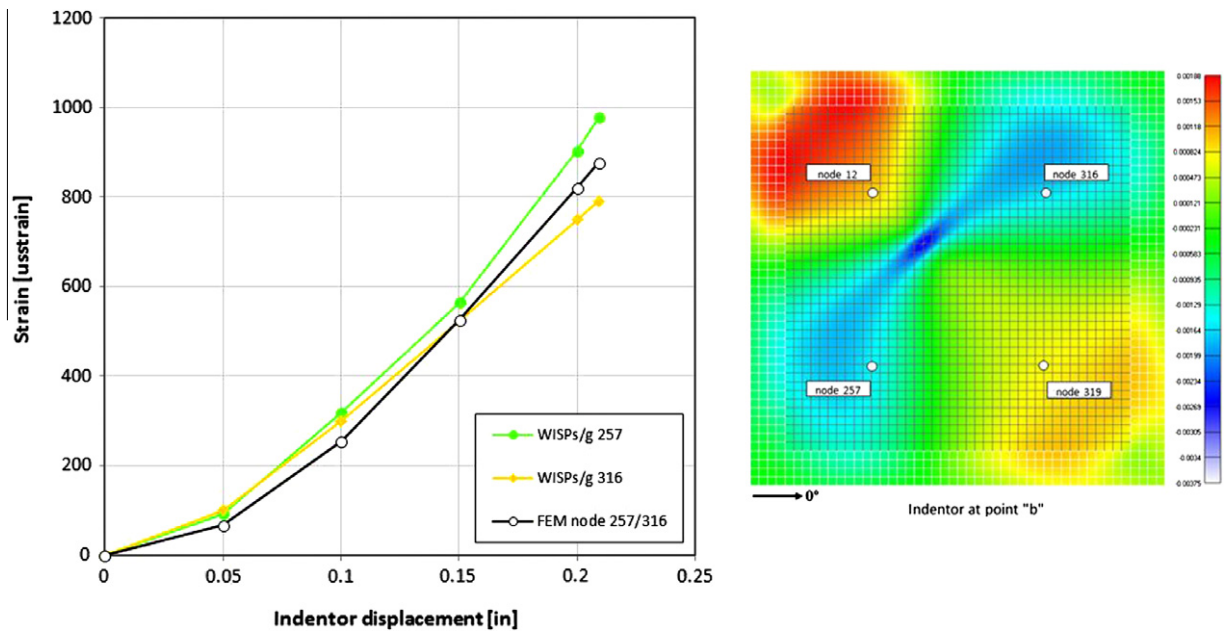


Fig. 18. (Left) Experimental and simulated strain curves for gages #257 and #316 as a function of indentor displacement for the load case (b). (Right) Strain contour plot from the simulation for the same load case. (For interpretation of the references to color in this figure legend, the reader is referred to the web version of this article.)

should generate an identical strain state in all four gages. Case (b) is an offset load, at 1.5 in. (38.1 mm) away from the center of the plate along one diagonal (45° from the 0 axis) in the direction of WISPs/g #12. This load case should generate a peak strain in the gage #12, a minimum in the most distant gage #319, and intermediate and equal strains in the two opposing gages #257 and #316. Case (c) is also an offset load at 1.5 in. (38.1 mm) away from the center of the plate, along the 90° axis of the plate. This load condition should generate an equal peak in gages #12 and #316, and an equal minimum in gages #257 and #319. The load is increased to 250 lb (1100 N) using step loads under displacement control. At each increment of 0.05 in. (1.27 mm), the load is held into place while the four values of strain are recorded.

Previous research [13–15] has shown that the strain field during such test is quite complex and cannot easily be predicted using closed form (plate theory) solutions. Therefore it is necessary to utilize a finite element model (FEM) approach. A NASTRAN model is generated using the nonlinear solver SOL106 and using CQUAD4 shell elements. Ply-by-ply stacking sequence is assigned using the nominal lamina elastic properties listed above in the experimental section. Element size is 0.25 in. (6.35 mm), for a total of 2401 elements and 2500 nodes, Fig. 15. For simplicity, elements are numbered so that the nodes that fall in the same location of the strain gages, have the same number as the WISPs/g strain gages. Boundary conditions are specified as simple supports, as mentioned previously, and load is applied as concentrated (nodal) force

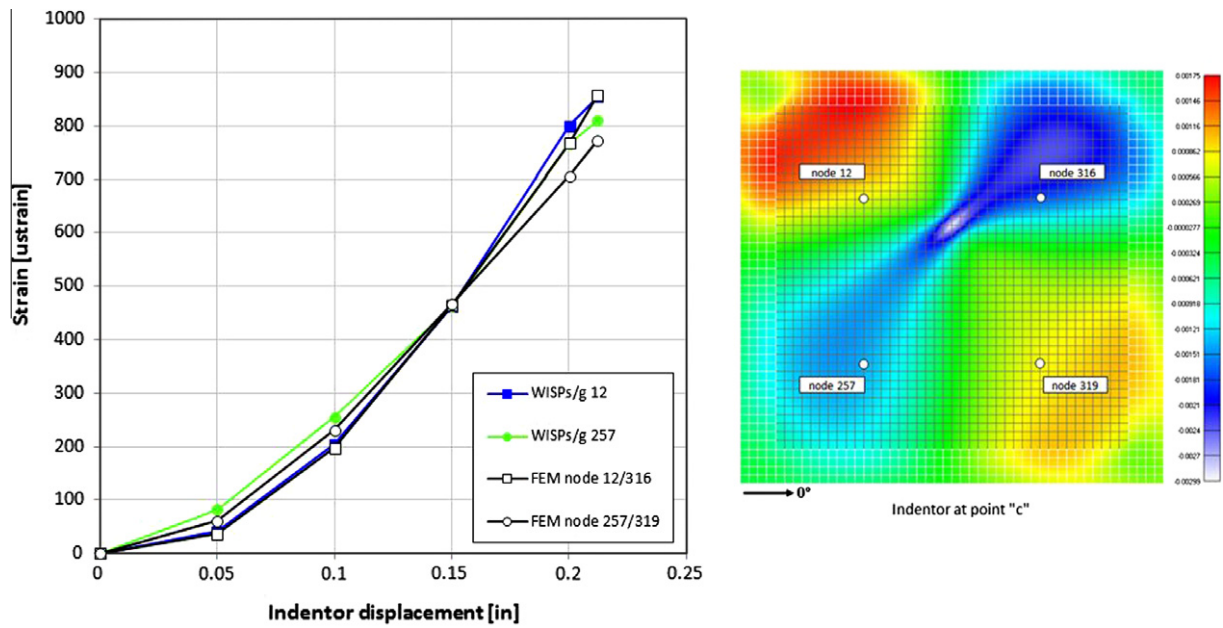


Fig. 19. (Left) Experimental and simulated strain curves for all four gages as a function of indentor displacement for the load case (c). (Right) Strain contour plot from the simulation for the same load case. (For interpretation of the references to color in this figure legend, the reader is referred to the web version of this article.)

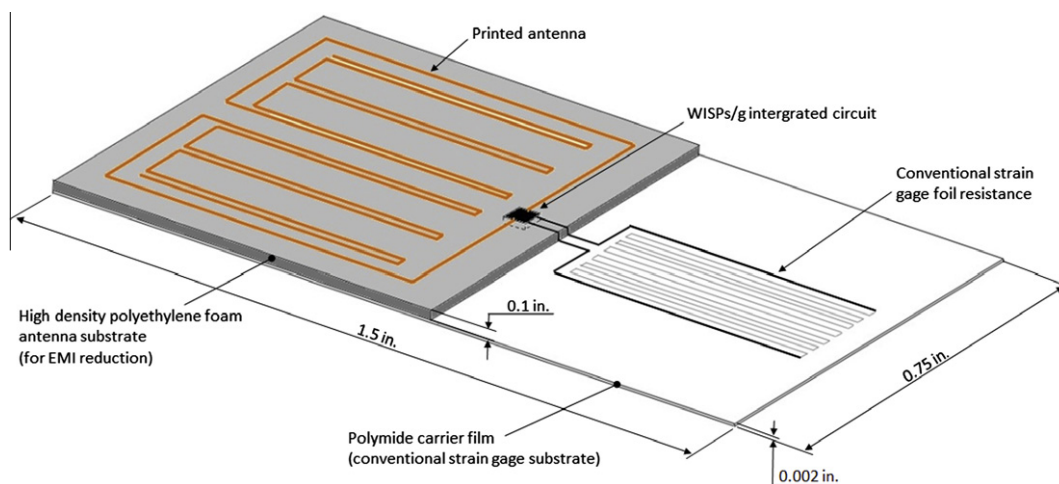


Fig. 20. Future development includes printing the WISPs/g into IC form. (For interpretation of the references to color in this figure legend, the reader is referred to the web version of this article.)

at each of the three locations described before. The assumption of using a single nodal force to model the contact load was verified for the case (a) of center-load only against a model that utilized a distributed constant pressure over an area of 0.25 in² (161 mm²). The midspan through-thickness deflection of the plate was used as metric for comparison and showed less than 1% difference between the two predictions. The convergence of the solution as a function of mesh size was also checked by refining the mesh size until the through-thickness deflection of the plate at midspan reached an asymptotic value (0.25829 in. or 6.56 mm), and such value was in agreement with the experimental measurement (0.26034 in. or 6.61 mm). The measurements obtained with all four WISPs/g devices are in good agreement with the FEM predictions given the complexity of the loading.

Results for the three load cases are shown in Figs. 16–19, and show the symmetric strain distribution of the centered indentation and the non-symmetric distributions of the offset indentations. For

each load case, the simulation prediction for the strain field in the 45° direction on the top ply (where the gages are situated) is shown, since the strain distributions on the top and bottom plies are significantly different. For load case (a), all four gage measurements are plotted along with a single FEM nodal prediction, Fig. 16. For load case (b), maximum and minimum strains at locations #12 and #319 are shown with the respective nodal predictions in Fig. 17, while in Fig. 18 the measurements at the equidistant gages #257 and #316 are plotted together with a single FEM prediction. Lastly, for load case (c), only two gage measurements are reported, since they are identical in pairs, together with the respective FEM prediction, Fig. 19. For load case (c), where the offset is not along the longitudinal direction of the gage but at 45° from it, the measurement is not as heavily influenced by the offset.

Following the successful completion of this stage of the research, which proves that the WISP technology can be utilized for acquiring and transmitting strain-gage measurements, further

work needs to be done to improve the packaging. The current WISPs/g platform is based on a bulky, heavy, and delicate PCB, which is suitable for research purposes since it can be easily modified in terms of hardware and firmware. Future developments will transfer the WISP into a commercial integrated circuit (IC) design. Such design can feature in a single-use (disposable), inexpensive package all WISPs/g components, including the antenna, the WISP platform, the interface circuit, and the pre-wired foil strain gage (Fig. 20). The IC tag will be manufactured using well-established electronic printing processes available in foundries worldwide. The compact IC tag will be based on a polyamide substrate 0.002 in. (0.05 mm) thick, identical to the carrier film used for conventional wired strain gages. Therefore, the tag will be bonded on the composite surface at the time of use using the traditional procedures for wired strain gages, such as surface abrasion and cleaning followed by liquid adhesive. The overall dimensions of the tag will be approximately 1.5 in. (38.1 mm) long and 0.75 in. (19.05 mm) wide for a strain gage of 0.5 in. (12.7 mm) effective length, Fig. 20. The reduction in the RF communication range due to the EMI of the carbon fiber substrate is the main concern, and further work will be aimed at developing a custom antenna that can improve the RF communication based on geometric and materials constraints. Approximately half of the IC tag will include an additional high density polyethylene (PET) film, approximately 0.1 in. (2.54 mm) thick. The PET substrate will act as the dielectric shield for the EMI and the base substrate for printing the WISPs/g antenna and circuitry. Applications of this technology in the IC configuration include strain measurement during structural static tests at the coupon, component and full-scale levels, as well as on-board real-time strain measurements during test flight and certification of new aircraft. Based on the experience developed on the strain measurement application, future research will expand to the development of a wireless temperature measurement device (WISPt/c), which will be based on conventional thermocouple sensor technology. Such device will be utilized to measure the temperature profile of the in situ patch cure for composite structural repairs.

5. Conclusions

The WISPs/g developed in this paper is based on the wireless, digital, battery-free platform patented by Intel and called WISP (Wireless Identification and Sensing Platform). The WISP was modified to interface with a conventional foil strain gage with the addition of a printed circuit board containing a Wheatstone bridge and amplifier. Demonstration of the technology was given through uniaxial tension tests, which showed that the strain measurement using the WISPs/g is repeatable and accurate as compared to traditional wired strain gages and extensometers. Final validation of the system was performed using four independent WISPs/g devices to

monitor the surface strain during a structural-level test. Non-linear, elastic FEA showed excellent agreement between the predictions and the WISPs/g measurements of strain during the quasi-static indentation of a square plate using a hemispherical indenter.

Acknowledgments

The WISP platform was developed at the Intel Research Labs in Seattle, WA. The tests were performed at the *Automobili Lamborghini* Advanced Composite Structures Laboratory in the Department of Aeronautics & Astronautics, College of Engineering, University of Washington. The authors would like to thank Maurizio Reggiani (VP & CTO of *Automobili Lamborghini S.p.A.*) and Dr. Al Miller (Boeing Commercial Airplanes, Technology Requirements and Incorporation) for supporting the study. The material used in this study was donated by Shreeram Raj, Cytec Engineered Materials.

References

- [1] Tata U, Deshmukh S, Chiao JC, Carter R, Huang H. Bio-inspired sensor skins for structural health monitoring. *Smart Mater Struct* 2009;18(10).
- [2] Jia Y, Sun K, Agosto FJ, Quinones MT. Design and characterization of a passive wireless strain sensor. *Meas Sci Technol* 2006.
- [3] Melik R, Perkoz NK, Unal E, Puttlitz C, Demir HV. Bio-implantable passive on-chip RF-MEMS strain sensing resonators for orthopaedic applications. *J Micromech Microeng* 2008;18(11).
- [4] Ko Wen H, Young DJ, Jun Guo, Suster M, Kuo Hung-I, Chaimanonart N. A high-performance MEMS capacitive strain sensing system. *Sens Actuat A: Phys* 2007;133/2:272–7.
- [5] Arms SW, Townsend CP, Galbreath JH, Newhard AT. Wireless strain sensing networks, 2nd European workshop on structural health monitoring. Munich, Germany; 2004.
- [6] Arms SW, Wood M, Swift S. Wireless strain measurement systems for aircraft test. Aerospace testing expo, Anaheim, CA; 2006.
- [7] Arms SW, Townsend CP, Churchill DL. Energy harvesting wireless sensors for helicopter damage tracking. In: Proceedings of AHS international forum 62, HUMS III session, Phoenix, AZ; 2006.
- [8] Arms SW, Townsend CP, Churchill DL, Galbreath JH, Corneau B, Ketcham RP, Phan N. Energy harvesting, wireless structural health monitoring and reporting system, 2nd Asia-Pacific workshop on SHM, Melbourne; 2008.
- [9] Sample AP, Yeager DJ, Powledge PS, Smith JR. Design of a passively-powered, programmable sensing platform for UHF RFID systems, In: IEEE international conference on RFID; 2007
- [10] Yeager DJ, Sample AP, Smith JR. WISP: a passively powered UHF RFID tag with sensing and computation. In: RFID handbook: applications technology security and privacy. CRC Press; 2008.
- [11] Chung DDL. Electromagnetic interference shielding effectiveness of carbon materials. *Carbon* 2001;39(2):279–85.
- [12] Tsotra P, Friedrich K. Electrical and mechanical properties of functionally graded epoxy-resin/carbon fibre composites. *Compos Part A: Appl Sci Manuf* 2003;34(1):75–82.
- [13] Feraboli P, Kedward KT. A new composite structures impact performance assessment program. *Compos Sci Technol* 2006;66(10):1336–47.
- [14] Feraboli P. Some recommendations for the characterization of the impact performance of composite panels by means of drop tower impact testing. *J Aircraft* 2006;43(6):1710–8.
- [15] Feraboli P. Forceful measures, energetic solutions. In: 21st ASC technical conference, Dearborn, MI; 2006.